




## REGULAR ARTICLE

### Green Synthesis of ZnO Nanoparticles Using Leaf Extracts of Tree Medicinal Plants from Togo and their Characterization and Antimicrobial Applications

E.S. Adewi<sup>1</sup>, K. Sesime<sup>1</sup>, A.D. Hounsi<sup>1</sup>, P. Pissang<sup>2</sup>, S.A.S. Bonou<sup>3</sup>, K.J.B. Amewotepe<sup>1</sup>, M. Agbahoungbata<sup>3</sup>, M.M. Dzagli<sup>1,4,\*</sup> , V.A. Adedeji<sup>5</sup>, A.C. Ahyi<sup>6</sup>, M.A. Mohou<sup>1</sup>

<sup>1</sup> Laboratoire LPMCS, Faculté Des Sciences, University of Lomé, 01BP1515 Lomé, Togo

<sup>2</sup> Laboratoire LaSBASE, ESTBA, University of Lomé, 01BP1515 Lomé, Togo

<sup>3</sup> Xrays Techniques Laboratory/Agence de Développement de Seme City X-TechLab, Seme, Bénin

<sup>4</sup> Centre d'Excellence Régional pour la Maîtrise de l'Electricité, University of Lomé, 01BP1515 Lomé, Togo

<sup>5</sup> Elizabeth City State University, USA

<sup>6</sup> Auburn University, National Coalition of Independent Scholars, USA

(Received 10 March 2025; revised manuscript received 20 June 2025; published online 27 June 2025)

Tropical infectious diseases develop resistance to antibiotics. The integration of nanoparticles in drugs could fight against this scourge. ZnO nanoparticle (ZnONPs) possesses remarkable antimicrobial properties, and their synthesis using medicinal plants is cost-effective and eco-friendly. The use of leaves of *newbouldias leavis*, *launaea taraxacifolia*, and *Combretum micranthum* in medicine was demonstrated in Togo, and their extract can be used as reducing and stabilizing agents of nanoparticles. This study evaluates the potential antimicrobial activities of ZnONPs, biosynthesized using leaf extracts of the three medicinal plants. The structural and optical properties of ZnONPs were investigated using UV-Vis, fluorescence, XRD, SEM, and EDS. The antibacterial potential of ZnONPs was assessed using two clinical and reference strains of *E. coli* and *S. aureus*. Spectroscopic measurements revealed an absorption peak between 370 and 377 nm, while the excitation at 365 nm produced spectra ranging from 450–700 nm. XRD analysis revealed a hexagonal wurtzite structure with a size of 39.05 nm. SEM analysis reveals nanostructures agglomerated, whereas EDS confirms the presence of ZnO. Antimicrobial tests against *S. aureus* and *E. coli* showed clear inhibition zones. Plant-based synthesis improves the biomedical properties of ZnONPs and constitutes a route for their use in nanomedicine.

**Keywords:** ZnO nanoparticles, Green synthesis, Structural and optical characterization, Antimicrobial application.

DOI: [10.21272/jnep.17\(3\).03004](https://doi.org/10.21272/jnep.17(3).03004)

PACS numbers: 81.07. – b, 87.85.Rs,  
78.67. – n, 81.16. – c

## 1. INTRODUCTION

The scientific community is interested in exploring and applying multifunctional nanomaterials in various fields. Their unique nanoscale properties, which depend on shape and size, make them attractive [1, 2]. Nanotechnology produces nanoparticles with distinctive characteristics such as low mass, large specific surface area, and high catalytic activity, as well as electrical, optical, antimicrobial, mechanical, and magnetic properties [3,4]. These properties have promoted advances in medicine, technology, and engineering [5]. Areas such as agriculture, with improved plant germination and growth [6], environment through wastewater purification [7], and energy, with improved yields of solar cells, have also benefited from nanotechnology [8].

Traditional synthesis methods of nanoparticles often use expensive and polluting physicochemical processes [9].

Physical methods require costly equipment and extreme conditions, while chemical methods involve harsh chemicals and waste, limiting their medical and food use [10]. The green synthesis of nanoparticles, using biosources, has emerged as an ecological and efficient alternative [11]. This method uses plants, microorganisms, and waste plants to create stable and multifunctional nanomaterials [12]. Infectious diseases pose a growing public health problem, exacerbated by the resistance of bacteria to conventional antibiotics due to their incorrect and excessive use, such as methicillin-resistant *Staphylococcus aureus* and vancomycin-resistant *Enterococcus* [10-13]. Infections caused by resistant bacteria, common in community and hospital settings, cost billions of dollars in healthcare [13]. Nanotechnology seems to be a safe avenue in the urgent search for new effective antimicrobial agents capable of killing and inhibiting the growth of microbes because its mechanism

\* Correspondence e-mail: [mdzagli@gmail.com](mailto:mdzagli@gmail.com)



of action is different from that of antibiotics [14]. Metal and metal oxide nanoparticles have been widely studied for their biological applications [15]. In particular, ZnO nanoparticles are distinguished by their characteristics such as a wide direct bandgap of 3.37 eV, high exciton binding energy of 60 meV, strong luminescence at room temperature, thermal stability, high mechanical and biocompatibility at room temperature biocompatibility and high photostability [16, 17]. ZnONPs possess excellent antibacterial, anti-fungal, photocatalytic, and antioxidant properties and applications in drug delivery, bioimaging, molecular diagnostics, and wound healing [8, 18]. Their good optical, electrical, and semiconductor properties made them ideal candidates for advanced solar cells and biosensors, electronic applications, optoelectronic applications, and laser technology, leading to important applications in many industries and research institutions [19, 21]. Traditionally, ZnONPs were fabricated by methods like hydrothermal, chemical vapor-liquid-solid deposition, metal-organic chemical vapor deposition, molecular beam epitaxy, sol-gel, microwave, laser ablation, chemical precipitation, and spray pyrolysis to meet high demand [19, 22]. Recently, biological synthesis using medicinal plant extracts has gained popularity due to its simplicity, low cost, safety, and environmental friendliness [2, 10, 21, 23]. Plant extracts are abundant, inexpensive, and contain many reducing and covering agents, favoring large-scale production [16].

In this study and to our knowledge, the leaf extracts of medicinal plants, notably *Newbouldia laevis*, *launaea taraxacifolia*, and *combretum micranthum*, commonly used in traditional medicine, were used for the first time for the synthesis of ZnONPs. *Newbouldia laevis* (*N. laevis*) often known as the 'African border tree' is an angiosperm that belongs to the family Bignoniaceae. Its average height is around 7 to 10 meters with numerous stems forming clumps of gnarled branches [24, 25]. *N. laevis* is a plant with many virtues. In sub-Saharan Africa, the different parts of *N. laevis* are used to treat various conditions. The bark is chewed to relieve stomach pain, diarrhea, and toothache. Stem bark decoctions treat epilepsy and convulsions in children, such as rheumatism, especially arthritis in the knee. The stems, leaves, and fruits are used as a febrifuge, dressing for wounds, and remedy for stomach ailments [26, 27]. Studies have shown that leaf and root extracts of *N. laevis* possess antimalarial and antimicrobial activities [28]. Evaluation of phytochemical constituents of *N. laevis* leaf extracts revealed the presence of ascorbic acid, vitamin E, saponins, alkaloids, cardiac glycosides, amino acids, vitamin A, steroids, tannins, terpenoids, and flavonoids [29] compounds involved in the reduction and capping of ZnONPs [17]. *Launaea taraxacifolia* (*L. taraxacifolia*) also called African lettuce is a tropical herb belonging to the Asteraceae family that can reach 150 cm high. The leaves of the *L. taraxacifolia* plant are consumed in West Africa either fresh in salads or cooked in sauce [30]. The use of *L. taraxacifolia* leaves in antioxidant and antiviral applications, in treating and controlling blood cholesterol levels, blood pressure, and

diabetes has been reported [31]. Previous work on leaves reported the presence of flavonoids, tannins, terpenoids, saponins, steroids, and bioactivities such as hypolipidemic, renoprotective, and hepatoprotective [32]. *Combretum micranthum* (*C. micranthum*), also known as "kinkéliba," belongs to the family of Combretaceae, a non-domesticated shrub found in the jungles of West Africa [33]. It is generally a shrubby species around 4-5 m in height. It is an ethnomedicinal plant widely used in West Africa in several treatment conditions, including diabetes mellitus and malaria fever [34]. These leaves are rich in polyphenols, including tannins, flavonoids, alkaloids, and others [35]. The extracts of these plants were used for the biosynthesis of ZnONPs, and the nanoparticles obtained were characterized by various spectroscopic and imaging techniques, before evaluating their anti-microbial activities against some pathogenic strains.

## 2. MATERIAL AND METHODS

### 2.1 Chemicals and Instrumentation

All acids and reagents used in this study are of analytical reagent grade. Zinc acetate dihydrate ( $\text{Zn}(\text{CH}_3\text{COO})_2 \cdot \text{H}_2\text{O}$ ) was purchased from DEAJUNG CHEMICALS & METALS Co. LTD, Korea (No. 8596-4405, CAS No. 5970-45-6). Sodium hydroxide, ethanol (99%), and distilled water were solvents. A refrigerator at 4°C, a magnetic stirrer coupled with a hot plate (0°C-310°C), a pHmeter (CHAUVIN ARNOUX Group / PSD1 pH METER), a Centrifuge (Biobase), a Whatmann filter paper, an oven and glassware (beakers, burette, Erlenmeyer flasks, a graduated cylinder), and BUCHI Rotavapor R-100, fitted with a B-100 water bath heating to 40°C, coupled to a vacuum pump V-100, were used.

### 2.2 Plant Material Collection and Extract Preparation

*N. Laevis*, *L. Taraxacifolia* and *C. Micranthum* leaves were selected as bio-reducing and stabilizing agents for this research. *N. Laevis* leaves were collected in April 2023 in a residence in Nyékonakpoè, Lomé, those of *L. Taraxacifolia* at the Gbossimé market in Lomé, and those of *C. micranthum* on the campus of the University of Lomé. All leaves were carefully washed with tap water and then distilled water to remove impurities before being stored at room temperature in the laboratory. They were then ground into powder using an electric mill for later use. Approximately 150 g of powder from each plant was introduced into 750 ml of distilled water (A), ethanol (B), and a hydroalcoholic solution (50 % water, 50 % ethanol) (C), respectively, for progressive maceration. The mixture was regularly stirred at 1500 rpm for 24 hours, and the contents of the vials were filtered using Whatmann No.1 filter paper to remove undissolved material. The obtained filtrates were stored in flasks and subjected to vacuum evaporation using a BUCHI Rotavapor to remove the solvent, thus obtaining solid extracts. The collected

extracts were stored in the refrigerator at 4°C for characterization and future use.

### 2.3 Green Synthesis of ZnONPs with Leaf Extracts

The green synthesis of ZnONPs was performed using the modified protocol from reference [36]. 500 mg of solid extracts are dissolved in 100 ml of initial solvent. Then, 80 ml of zinc acetate dihydrate solution (1M) was mixed with 20 ml of each extract (5 mg/ml). The initial pH of the mixture is measured, then stirred at 500 rpm for 2 hours at room temperature. The pH is then adjusted to 11, the optimal pH for synthesizing ZnONPs, by adding dropwise a sodium hydroxide solution (2M). The mixture is then stirred vigorously at 1500 rpm for 1 hour, until a white precipitate forms at the bottom of the beaker. The supernatant is decanted, and the white precipitate is washed several times with distilled water, then centrifuged at 3000 rpm for 15 minutes. After centrifugation, the white precipitate is collected, filtered, and dried in a vacuum oven at 60 °C. Finally, the dried product is calcined in an oven at 400 °C for 1 hour to obtain the ZnONPs. ZnONPs were successfully obtained using aqueous, ethanolic, and hydroethanolic leaf extracts of *N. Leavis* (NL-ZnONPs), *L. Taraxacifolia* (LT-ZnONPs), and *C. Micranthum* (CM-ZnONPs), respectively.

### 2.4 Structural and Morphological Characterization

The biosynthesized ZnONPs were first characterized by UV-Vis spectroscopy. The ZnONP powders were dispersed in sodium hydroxide. The UV-Vis spectrophotometer (UV-5200PC, SHANGHAI METASH INSTRUMENTS, Co. LTD) of the Chemistry Department of the University of Lomé was used to measure the absorption spectra and to detect the maximum surface plasmon resonance in the wavelength range of 190 to 600 nm. The bandgap energy ( $E_g$ ) of the ZnONPs was calculated using the Eq. (1):

$$E_g = \frac{hc}{\lambda} \quad (1)$$

where  $h$  is Planck's constant ( $6.626 \times 10^{-34}$  J.s),  $c$  is the speed of light in a vacuum ( $3 \times 10^8$  m/s) and  $\lambda$  is the wavelength corresponding to the absorption peak. It is generally agreed that UV-Vis spectroscopy can evaluate nanoparticles of controlled size and shape in aqueous suspensions [37, 38]. The average particle size can be determined from the maximum absorption wave-length of the effective mass model described by the Brus Eq. (2) [39]:

$$E = E_g^{bulk} + \frac{\hbar^2 \pi^2}{2er^2} \left( \frac{1}{m_0 m_e^*} + \frac{1}{m_0 m_h^*} \right) - \frac{1.8e}{4\pi r \epsilon \epsilon_0} - \frac{0.124e^3}{\hbar^2 (4\pi \epsilon \epsilon_0)^2} \left( \frac{1}{m_0 m_e^*} + \frac{1}{m_0 m_h^*} \right)^{-1} \quad (2)$$

where  $E_g^{bulk}$  is the bandgap energy (eV) of bulk ZnO,  $\hbar$  is Plank's constant,  $r$  is the radius of the particle,  $m_e$ ,  $m_h$  and  $m_0$  are respectively the effective mass of the electron, the hole, and the free electron,  $e$  is the charge on the electron,  $\epsilon$  is the relative permittivity, and  $\epsilon_0$  is

the permittivity of vacuum. Due to relatively low effective masses of ZnO ( $m_e = 0.26$ ,  $m_h = 0.59$ ), a wide band gap is expected for particle radii below about 4 nm. After the derivation of Eq. (2) and with a mathematical simplification, Eq. (3) was obtained to find the particle size from the absorbance spectra [40].

$$r \text{ (nm)} = \frac{-0.3049 + \sqrt{-26.23012 + \frac{10240.72}{\lambda_p \text{ (nm)}}}}{-6.3829 + \frac{2483.2}{\lambda_p \text{ (nm)}}}, \quad (3)$$

where  $\lambda_p$  is the maximum wavelength.

The fluorescence spectra of the different samples of ZnONPs powder dissolved in sodium hydroxide were obtained at an excitation wavelength of 365 nm using the SILVER-Nova spectrophotometer (StellarNet, USA) of the Laboratoire de Physique des Matériaux et des Composants à Semi-Conducteurs at the University of Lomé.

The crystal structure of ZnONPs was determined using the Malvern Panalytical Empyrean Alpha 1 X-ray diffractometer with Cu-K $\alpha$  radiation at the Seme City X-TechLab X-ray Techniques Laboratory/Development Agency (Benin). The analysis was carried out over a 2 $\theta$  range from 3° to 70° at 0.01° steps with a voltage of 45 KV and a current of 40 mA. The Debye-Scherrer equation stated as Eq. (4) was used to calculate the average crystallite size (nm) [11].

$$D = \frac{k\lambda}{\beta \cos \theta}, \quad (4)$$

where  $D$  is the average size of the crystal particles,  $\lambda$  is the X-ray wavelength (0.15406 nm),  $k$  is the Scherrer constant (0.94),  $\theta$  is the Bragg diffraction angle, and  $\beta$  is the full width at half maximum of the XRD peak.

The morphology analysis of different ZnONPs was examined using JEOL JSM 6010PLUS/LA Analytical Scanning electron Microscope from Elizabeth City State University in North Carolina (USA). To obtain the images, the nanoparticle powders were added to a silicon slide attached with carbon tape and measured at an accelerating voltage of 20 kV. The elemental composition of nanoparticles was determined using the Energy-dispersive X-ray spectroscopy (EDS) connected to the SEM.

### 2.5 Antimicrobial Analysis

The microorganisms used in this study consisted of clinical strains isolated from the medical bacteriology laboratories of the campus and Sylvanus OLYMPIO University Hospital Centers and the National Institute of Hygiene (INH) of Lomé and reference strains. The clinical strains were mostly isolated from urine and salts. These are Gram-negative bacteria, *Escherichia coli* (E. coli), Gram-positive bacteria, *Staphylococcus aureus* (S. aureus), *Enterococcus*, and yeast, *Candida albicans* (C. albicans). The reference strains concerned *S. aureus* ATCC 29213, *E. coli* 25922, and *C. albicans* ATCC 14053. These are strains recommended by the

“National Committee for Clinical Laboratory Standards” (NCCLS) for sensitivity studies. Most species in this study are frequently implicated in gastroenteritis and urinary infections. All strains were cultured at 37°C for 18 to 24 hours and preserved by successive subcultures throughout the study.

The bacteria were cultured in Muller Hinton broth (Liofilchem, Italy) for 24 hours so that they were in the exponential growth phase. Each culture was then suspended in sodium chloride saline solution (0.9 % NaCl) at a turbidity equivalent to that of the 0.5 Mac Farland scale standard. This suspension, with an optical density of less than 0.5 at 625 nm, corresponds to  $1$  to  $2 \times 10^6$  CFU/ml and will be an inoculum for the tests [41].

The dehydrated Mueller Hinton agar (MHA) medium (Liofilchem, Italy) was suspended in distilled water at 36 g/l and then heated in a water bath until completely dissolved. The pH was adjusted to  $7.3 \pm 0.1$ , and the medium was sterilized in an autoclave at 120 °C for 15 minutes. It was then cooled to 45 to 50 °C and poured into sterile Petri dishes of 90 mm in diameter so that the thickness was equal to 4 mm [41].

Evaluation of the antimicrobial activity of ZnONPs synthesized based on aqueous, alcoholic, and hydroalcoholic extracts of *N. Laevis*, *L. Taraxacifolia*, and *C. Micranthum* was carried out by the diffusion method on agar medium (Mueller- Hinton Agar) or well method. The extracts to be tested were prepared at the initial concentration of  $C_0 = 200$  mg/ml. The microbial suspensions (inoculum) in the exponential growth phase (0.5 on the McFarland scale, or approximately  $1.5.10^6$  cells/ml) were inoculated by flooding on sterile Mueller-Hinton Agar. After drying the plates, 5 to 6 mm diameter holes were made concentrically on each culture medium. 50  $\mu$ l (10 mg/ml) of distinct ZnONPs is introduced into each well. The reference drugs (positive controls) and the solvent (distilled water) are treated under the same conditions. After 15 minutes of pre-diffusion at room temperature, the boxes are incubated at 37°C (bacteria and yeast) for 24 hours, at the end of which the diameters of the growth inhibition zones are measured using a compass and a double decimeter. The tests are repeated twice, and the results are recorded as the average diameter of the two experiments [42].

### 3. RESULTS AND DISCUSSION

#### 3.1 Formation of Zinc Oxide Nanoparticles

Fig. 1 presents the color change of the reaction medium as the first crucial indicator of the formation of biosynthesized ZnONPs.

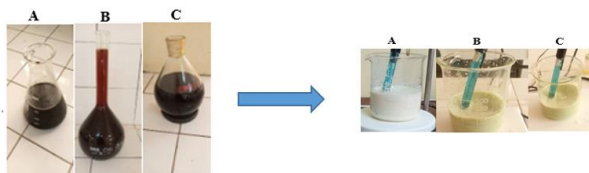


**Fig. 1** – Formation of zinc oxide nanoparticles

The leaf extract color was changed to cloudy white after adding zinc acetate and adjusting the pH using sodium hydroxide solution.

#### 3.2 UV-Vis and Fluorescence Spectroscopy Analysis

Fig. 2 presents UV-visible and fluorescence spectra of the successful biosynthesis of ZnONPs. The spectra showed significant peaks (from 370 to 375 nm) for NL-ZnONPs, LT-ZnONPs, and CM-ZnONPs, respectively, as depicted in Table 1, which indicates a coupled vibration of the electrons of the nanoparticles with the light waves [43]. Table 1 summarizes the peak absorbance wavelengths, band gap energy, and the sizes of the nanoparticles in colloidal suspension and powder forms using XRD.

High absorption bands observed could also be attributed to the inherent bandgap absorption of ZnO caused by electronic transitions from the valence band maximum ( $O_{2p}$ ) to the conduction band minimum ( $Zn_{3d}$ ) [44]. The present results are similar to previous studies that evaluated the suitability of the aqueous extract of leaves from *croalaria verrucosa* [45], *Artemisia annua* [36] to produce ZnONPs with a maximum absorption of 375 nm. Furthermore, obtaining unique peaks on each spectrum reveals that the biosynthesized ZnONPs are pure [46]. Different values of the bandgap energy for ZnONPs as given in Table 1 reveal that the nature of the extract affects the bandgap of nanoparticles. The significant UV absorptions by ZnONPs would have multiple biomedical applications for example sunscreen protectors against the negative effects of UV rays and antibacterial ointments [13, 46].

The fluorescence spectra of the different ZnONPs samples (Fig. 2) showed a broad, stable, and strong emission band in the visible range (450 – 700 nm). This can be explained by the emission due to structural vacancies, such as oxygen or zinc interstitials [36, 47]. These results could be used to optimize the properties of ZnONPs for specific applications, such as optoelectronic devices, sensors, and photocatalysts [48].

#### 3.3 X-ray Diffraction Analysis

Fig. 3 presents the diffractogram of the ZnONPs corresponding to the intensity of the diffracted x-rays as a function of the diffraction angles. The sharp diffraction peaks were found at  $2\theta$  values of 31.76; 34.42; 36, 25; 47.54; 56.59; 62.86; 66.40; 68.08, and 69.08 as-signed, respectively, to the (*hkl*) values of (100), (002), (101), (102), (110), (103), (200), (112), and (201) in the investigation. The intense peak in the (101) direction of the diagrams confirmed the well-crystallized hexagonal wurtzite structure of the biosynthesized ZnONPs [36]. The sizes of the different ZnONP particles calculated using formula (4) are recorded in Table 1. These results agreed with those validating the crystalline structure of nanoparticles, showing similar peaks for ZnONPs obtained from various extracts of *Veronica multifida* [49] and *dysphania ambrosioides* [50].

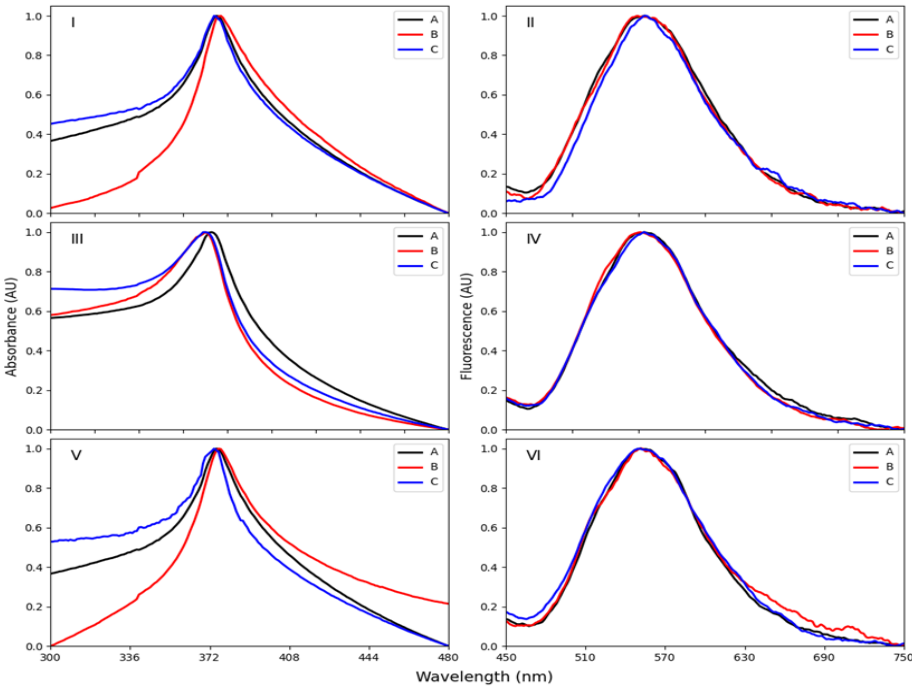
### 3.4 Scanning Electron Microscopy and Energy Dispersive Spectroscopy (EDX)

Fig. 4 presents the scanning electron microscopy (SEM) images of the obtained ZnONPs prepared using aqueous, alcoholic, and hydroalcoholic extracts. The SEM analysis was carried out to determine the morphology of the nanoparticles. The SEM images showed several rough aggregations of nanoparticles due to the bonds with plant extracts. The micrograph showed that the biosynthesized ZnONPs are spherical, as previously reported by Akhter et al. [51]. The compact morphology of the agglomerated nanoparticles can be attributed to heat in the electric furnace, which gives the crystal-line nature [52]. Fig. 5 presents energy dispersive X-ray (EDS) spectra of ZnONPs

biosynthesized by aqueous, alcoholic, and hydroalcoholic extracts. The analysis reveals that zinc and oxygen are in high concentration, while carbon, silicon, chlorine, and sulfur are in trace amounts. The presence of strong peaks of zinc and oxygen between 0 and 2 keV and between 8 and 10 keV confirms the presence of zinc oxide nano-particles using the three plant extracts. The traces of carbon, silicon, chlorine, and sulfur observed in the spectra would come from the involvement of photo-chemical groups, carbon tape used as a fixing base, or the slide on which the powders were deposited. Similar results were obtained during the biosynthesis of ZnONPs via the alcoholic extract of *Artemisia annua* [36] and aqueous extract of *calotropis gigantea* [53].

**Table 1** – Peak absorbance wavelength, band gap energy, colloidal, and powder particle sizes

Particles		Peak absorbance wavelength $\lambda_p$ (nm)	Band gap energy $E_g$ (eV)	Particle size in colloidal (nm)	Size (nm)
NL-ZnONPs	A	375	3.31	6.46	33.21
	B	377	3.29	6.48	44.33
	C	374	3.32	5.98	41.60
LT-ZnONPs	A	375	3.31	6.46	41.60
	B	370	3.35	5.46	33.21
	C	370	3.35	5.46	39.17
CM-ZnONPs	A	371	3.34	5.58	37.01
	B	377	3.29	6.48	37.01
	C	374	3.32	5.98	44.34



**Fig. 2** – UV-visible and fluorescence spectra of zinc oxide nanoparticles synthesized using aqueous (a), alcoholic (b), and hydroalcoholic (c) extracts of *N. Leavis* (I, II), *L. Taraxacifolia* (III, IV) and *C. Micranthum* (V, VI)



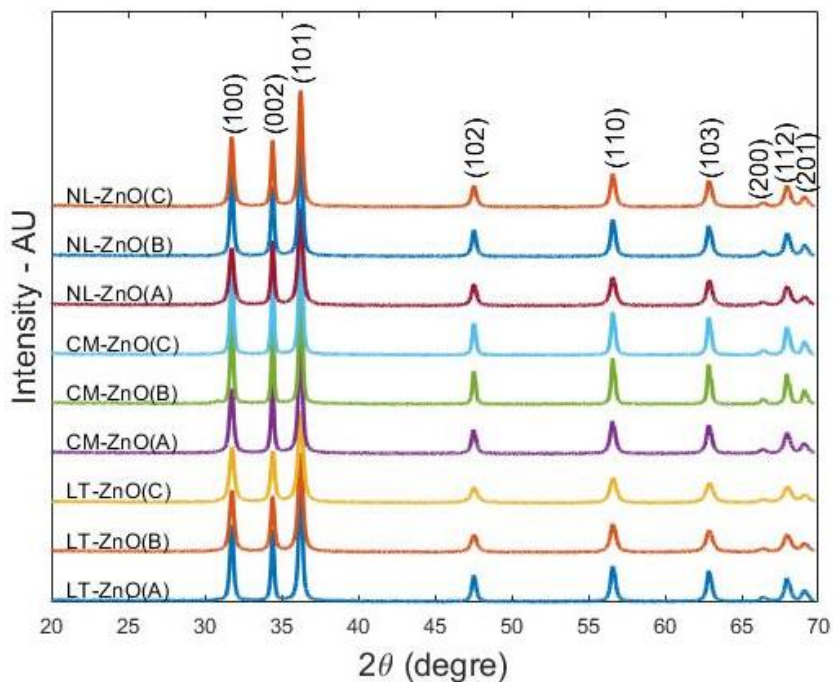


**Fig. 3** – X-Ray diffraction patterns for zinc oxide nanoparticles synthesized using aqueous (A), alcoholic (B), and hydroalcoholic (C) extracts of *L. Taraxacifolia*, and *C. Micranthum*, and *L. Leavis*

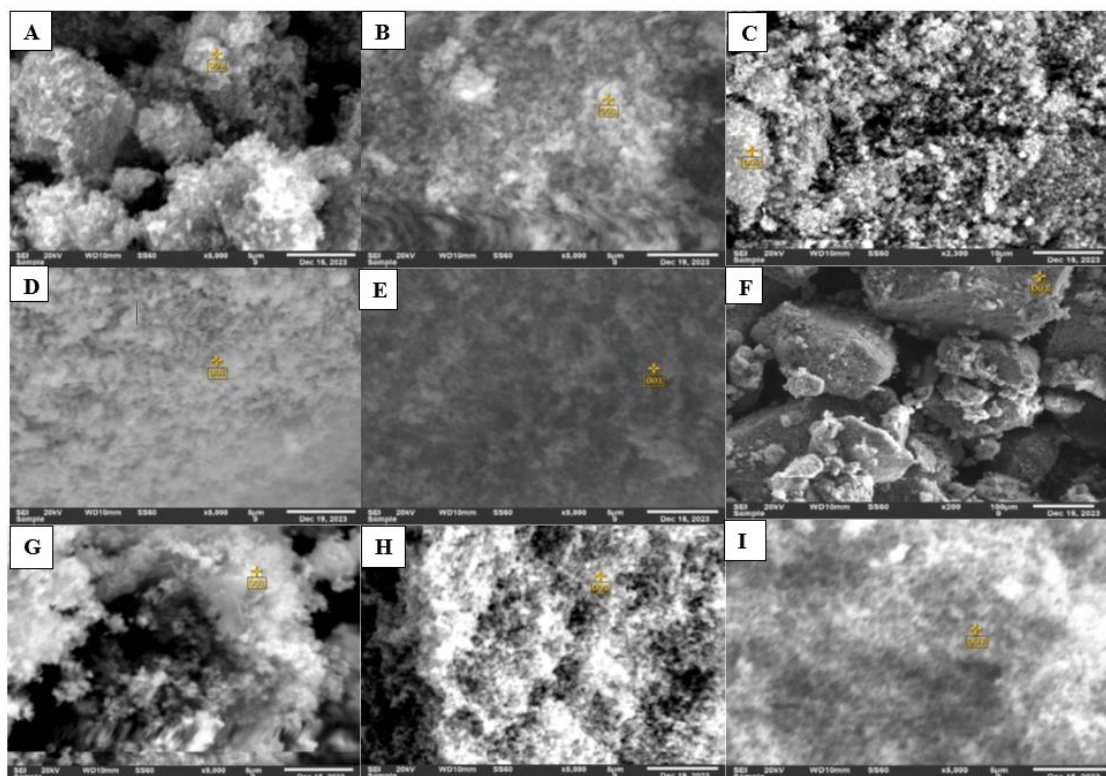


**Fig. 4** – SEM images of ZnONPs synthesitised using respectively aqueous, alcoholic and hydroalcoholic extracts newbouldias leavis (A, B, C), launaea taraxacifolia (D, E, F) and combretum micranthum (G, H, I)

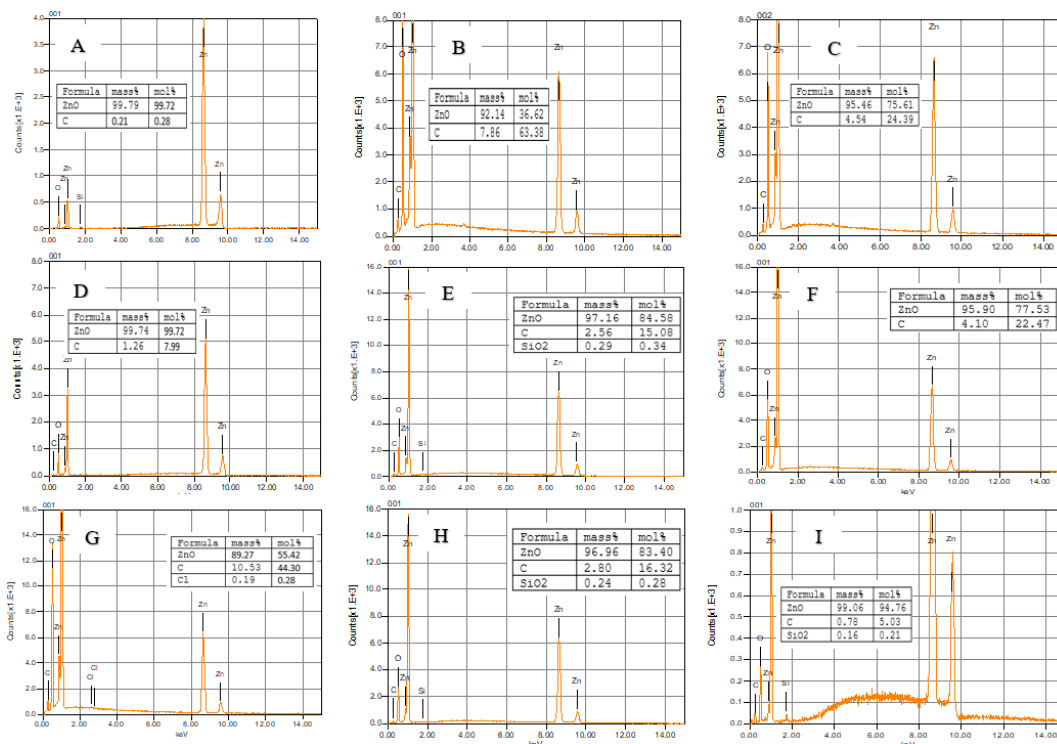


**Fig. 5** – EDX spectra of ZnONPs synthesized using respectively aqueous, alcoholic, and hydroalcoholic extracts of newbouldias leavis (A, B, C), launaea taraxacifolia (D, E, F) and combretum micranthum (G, H, I)

### 3.5 Antimicrobial Activity

The disk diffusion method was used to evaluate antibacterial activities. Although it confirms the efficacy of ZnO nanoparticles, this approach does not allow us to accurately determine the minimum inhibitory concentration (MIC) or explore the toxicity mechanisms of nanoparticles against pathogens. Nevertheless, it re-mains a simple, effective, and practical method for verifying the antibacterial properties of a sample [54]. The present study, therefore, focuses exclusively on confirming the antibacterial activity of biosynthesized ZnO nanoparticles.

Fig. 6 presents the diameter of the zones of inhibition of the antibacterial activity of ZnONPs obtained via the extract of *N. Leavis* (Fig. 6-I and II), *L. Taraxacifolia* (Fig. 6-III and IV), and *C. Micranthum* (Fig. 6-V) against the two clinical and reference strains of *E. Coli* and *S. Aureus*, and *C. Albicans*. ZnONPs had antibacterial activity against the two clinical and reference strains of *E. Coli* and *S. Aureus* and had no action on *C. Albicans*. The ZnONPs via the *C. Micranthum* (Fig. 7-V) extract reacted only with the *S. Aureus* strains as indicated by the diameter of the inhibition zones.

Standard antibiotics such as nystatin against *C. Albicans*, vancomycin against *S. Aureus*, and norfloxacin against *E. Coli* have shown inhibitory activity against the pathogens. Distilled water was used as a negative control. Using NL-ZnONPs showed a maximum inhibition zone of 15 mm and 13 mm against clinical and reference strains of *E. Coli* for the concentration 200 mg/ml; 20 mm, and 16 mm for the

clinical and reference strains of *S. Aureus* for 200 mg/ml. LT-ZnONPs exhibited 15 mm inhibition for clinical strains of *E. Coli* at 200 mg/ml, 13 mm for the *E. Coli* reference at 100 mg/ml, and 19 mm for the clinical strain of *S. Aureus* at 100 mg/ml, and 19 mm for the reference strain of *S. Aureus* for 200 mg/ml. Finally, an inhibition of 19 mm and 12 mm of CM-ZnONPs on the clinical and reference strains of *S. Aureus* was observed for 200 mg/ml. The present study revealed that the reference strains were less sensitive than the clinical strains due to the nature of the pathogens. It is also noted that Gram-positive bacteria (*S. aureus*) were more sensitive to the biosynthesized ZnONPs than Gram-negative bacteria (*E. Coli*). The results obtained are in good agreement with those reported in previous studies, in which it was observed that ZnONPs were more active against Gram-positive bacteria (*S. aureus* and *Bacillus subtilis*) than Gram-negative bacteria (*E. Coli* and *Pseudomonas aeruginosa*) [55]. The findings generally revealed the dose-dependent effect of ZnONPs, because the increase in the concentration of the nanoparticles led to an increase in the antibacterial activity exerted by the nanoparticles, and were similar to the work of Ifeanyichukwu et al. [40].

The mechanisms and efficacy of the antibacterial activities of ZnO nanoparticles were well-documented in the literature [56]. These mechanisms include the formation of free radicals, such as singlet oxygen, hydrogen peroxide ( $H_2O_2$ ), hydroxyl radicals, and  $Zn^{2+}$  ions. These reactive species, released from the surface of

nanoparticles, play a crucial role in inhibiting bacterial growth. Indeed, they cause significant damage to the bacterial cell wall, compromise DNA integrity, and generate pores within the cell membrane, leading to an inability of bacteria to survive in their environment [54,

57]. In addition, the activation of ZnO by ultraviolet (UV) and visible light determines its antibacterial activity. This activation generates electron-hole pairs, which contribute to the oxidation of essential biomolecules and the destabilization of bacterial membranes.

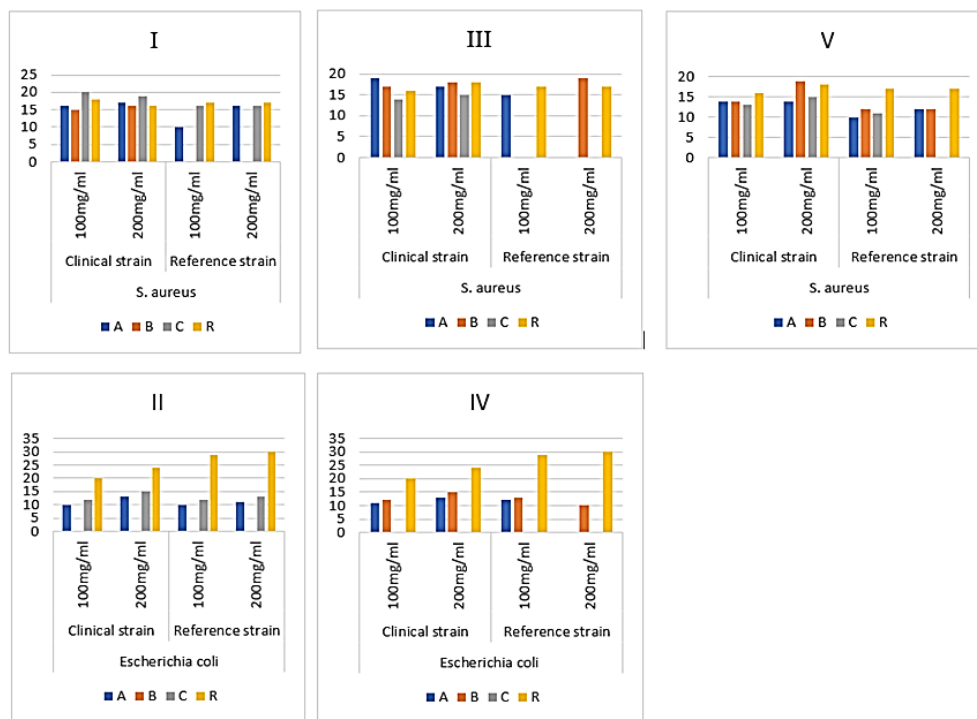


**Fig. 6** – Diameter (mm) of zones of inhibition of ZnONPs on clinical and reference strains of *E. Coli* of *S. Aureus*

Studies have shown that these interactions make ZnONPs particularly dangerous for the bacterial strains tested, revealing their effectiveness as antibacterial agents [58, 59]. These properties give ZnO nanoparticles considerable potential in various fields, such as commercial and medical applications [54]. Their ability to act against bacteria makes them ideal candidates for health and beauty care products. Indeed, biosynthesized ZnO nanoparticles can be effectively incorporated into skin care formulations, ointments, and cosmetics to provide antibacterial benefits and soothing and protective effects [60].

#### 4. CONCLUSION

The green synthesis of ZnONPs via plant extract has generated considerable enthusiasm due to its inexpensive protocol and environmentally friendly nature. In this study, aqueous, ethanolic, and hydroethanolic extracts were successfully used for ion zinc reduction to ZnONPs. The biosynthesized samples were characterized using UV-visible and fluorescence spectroscopy, XRD, SEM, and EDX. The results showed the successful synthesis of spherical ZnONPs with a hexagonal wurtzite structure. The biosynthesized ZnONP antimicrobial activities depended on the dose

and nature of the extract. The biosynthesized ZnONPs were more sensitive to Gram-positive bacteria than to Gram-negative bacteria. The obtained data confirm the high efficiency of the three plants as a biocatalyst for the green synthesis of ZnONPs for integration in different biomedical applications. Further research on ZnONPs should pave the way for innovations in healthcare and cosmetics, enabling safer and more effective solutions for fighting infections while improving the quality of products.

#### AKNOWLEDGEMENTS

The authors acknowledge the “Laboratoire de Physique des Matériaux et des Composants à Semi-conducteurs” at the University of Lomé. The authors are grateful for the financial support from the International Science Program (ISP, Uppsala) through a grant to the African Spectral Imaging Network (AFSIN). The authors gratefully acknowledge the support of X-TechLab, the experiment platform dedicated to X-ray techniques for scientific and technological research, hosted by the Agence de Développement de Sèmè City in Benin. The authors thank the staff of the “Centre d’Excellence Régional pour la Maîtrise de l’Electricité (CERME)”, at the University of Lomé for the support.



## REFERENCES

1. A. Fouda, E. Saied, A.M. Eid, F. Kouadri, A.M. Alemam, M.F. Hamza, M. Alharbi, A. Elkelish, S.E.D. Hassan, *J. Funct. Biomater.* **14**, 205 (2023).
2. B. Elzein, *Heliyon* **10** No 10, e31393 (2024).
3. G.K. Prashanth, M.S. Dileep, M. Gadewar, M.K. Ghosh, S. Rao, A.S. Giresha, P.A. Prashanth, M.M. Swamy, K.V. Yatish, M. Muttharaju, *BioNanoSci.* **14**, 1876 (2024).
4. V. Jadhav, A. Roy, K. Kaur, A.K. Rai, S. Rustagi, *Nano-Struct Nano-Objects* **37**, 101103 (2024).
5. T. Karan, Z. Gonulalan, R. Erenler, U. Kolemen, O. Eminagaoglu, *J. Mol. Struct.* **1296**, 136836 (2024).
6. D. Asmat-Campos, E. López-Medina, G. Montes de Oca-Vásquez, E. Gil-Rivero, D. Delfín-Narciso, L. Juárez-Cortijo, R. Rafael-Amaya, *Molecules* **27** No 7, 2343 (2022).
7. S.M. Abegunde, M.A. Adebayo, E.F. Olasehinde, *Green Energy Res.* **2** No 2, 100073 (2024).
8. X. Yang, X. Cao, C. Chen, L. Liao, S. Yuan, S. Huang, *Separations* **10** No 9, 466 (2023).
9. S. Azizi, M.B. Ahmad, F. Namvar, R. Mohamad, *Mater. Lett.* **116**, 275 (2014).
10. E.I. Muresan, A. Pui, C. Cernatescu, R. Cimpoesu, C.E. Horhoge, B. Istrate, C.M. Rimbu, *Appl. Sci.* **14** No 11, 4612 (2024).
11. S.J. Sugitha, R. Venkatesan, R.G. Latha, A.A. Vetcher, B.A. Al-Asbahi, S.C. Kim, *Molecules* **29** No 7, 1464 (2024).
12. N. Bhattacharjee, I. Som, R. Saha, S. Mondal, *Int. J. Environ. Anal. Chem.* **104** No 3, 489 (2024).
13. M.H. Morowvat, K. Kazemi, M.A. Jaber, A. Amini, A. Gholami, *Materials* **16** No 2, 842 (2023).
14. A. Salayová, Z. Bedlovičová, N. Daneu, M. Baláz, Z. Lukáčová Bujňáková, L. Balázová, L. Tkáčiková, *Nanomaterials* **11** No 4, 1005 (2021).
15. Zeghoud, S., Hemmami, H., Seghir, B. B., Amor, I. B., Kouadri, I., Rebiai, *J. Mater. Today Commun.* **33**, 104747 (2022).
16. S.T. Karam, A.F. Abdulrahman, *Photonics* **9** No 8, 594 (2022).
17. T.R. Acharya, P. Lamichhane, R. Wahab, D.K. Chaudhary, B. Shrestha, L.P. Joshi, E.H. Choi, *Molecules* **26** No 24, 7685 (2021).
18. T.T. Truong, T.T. Khieu, H.N. Luu, H.B. Truong, V.K. Nguyen, T.X. Vuong, T.K.N. Tran, *Materials* **16** No 15, 5457 (2023).
19. H. Ahmad, K. Venugopal, K. Rajagopal, S. De Britto, B. Nandini, H.G. Pushpalatha, S. Jogaiah, *Biomolecules* **10** No 3, 425 (2020).
20. N. Sedefoglu, *Ceram. Int.* **50** No 6, 9884 (2024).
21. S.A. Akintelu, A.S. Folorunso, *BioNanoSci.* **10** No 4, 848 (2020).
22. M. Rafique, R. Tahir, S.S.A. Gillani, M.B. Tahir, M. Shakil, T. Iqbal, M.O. Abdellahi, *Int. J. Environ. Anal. Chem.* **102** No 1, 23 (2022).
23. I. Ayoub, V. Kumar, R. Abolhassani, R. Sehgal, V. Sharma, R. Sehgal, Y.K. Mishra, *Nanotechnol. Rev.* **11** No 1, 575 (2022).
24. F.T. Bothon, M. Moustapha, G. SophieBogninou, C.P.A. Dossa, B. Yehouenou, S.E. Medoatinsa, D.C. Sohounhloué, *Bull. Env. Pharmacol. Life Sci.* **3** No 11, 09 (2014).
25. E. Bafor, U. Sanni, *Indian J. Pharm. Sci.* **71** No 2, 124 (2009).
26. S.I. Egba, G.I. Sunday, E.G. Anaduaka, *J. Pharm. Biol. Sci.* **9** No 3, 61 (2014).
27. R.J. Ogbe, C.D. Luka, G.I. Adoga, *Clin. Phytosci.* **6**, 28 (2020).
28. L.A. Okeke, C.O. Anie, D.C. Nwobodo, V.K. Okolo, *GSC Biol. Pharm. Sci.* **22** No 3, 144 (2023).
29. S.A. James, A. Sunday, A. Jonah, A.P. Ojonugwa, A.O. Victoria, *Saudi J. Pathol. Microbiol.* **2** No 6, 192 (2017).
30. O. Koukoui, P. Agbangnan, S. Boucherie, M. Yovo, O. Nusse, L. Combettes, D. Sohounhloué, *Am. J. Plant Sci.* **6** No 11, 1768 (2015).
31. M.S. Owolabi, A.L. Ogundajo, A.O. Alafia, K.O. Ajelara, W.N. Setzer, *Foods* **9** No 7, 914 (2020).
32. M.B. Adinortey, C. Ansah, A. Weremfo, C.A. Adinortey, G.E. Adukpo, E.O. Ameyaw, A.K. Nyarko, *J. Nat. Sci. Biol. Med.* **9** No 1, 6 (2018).
33. S. Hu, J.E. Simon, M. Wang, Y. Wu, Y. Huang, Q. Wu, *Molecules* **28** No 4, 1791 (2023).
34. M.Y. Beda, V. Besson, S. Beourou, K. Koffi, *Afr. J. Food Sci. Res.* **2**, 37 (2014).
35. A. Chika, S.O. Bello, *J. Ethnopharmacol.* **129** No 1, 34 (2010).
36. K. Sesime, M.M. Dzagli, K.B.R.J. Afoudji, *J. Optoelectron. Biomed. Mater.* **13** No 4, 193 (2021).
37. S. Ahmed, M. Ahmad, B.L. Swami, S. Ikram, *J. Radiat. Res. Appl. Sci.* **9** No 1, 1 (2016).
38. M.S. Samuel, Lekshmi Bose, K.C. George, *Acad. Rev.* **16**, 57 (2009).
39. S. Singh, J.V. Gade, D.K. Verma, B. Elyor, B. Jain, *Opt. Mater.* **152**, 115422 (2024).
40. S. Talam, S. R. Karumuri, N. Gunnam, *Int. Schol. Res. Not.* **2012** No 1, 372505 (2012).
41. P.Y. Hoekou, T. Tchacondo, K.A. Gbogbo, D. Tchelougou, P. Pissang, S.D. Karou, B. Faso, *Int. J. Curr. Microbiol. App. Sci.* **4** No 5, 882 (2015).
42. S. Effoe, A. Agban, Y. Hoekou, K.A. Dakey, I. Kpabi, H.E. Gbekley, P. Pissang, T. Tchacondo, *Int. J. Innov. Stud.* **30**, 239 (2020).
43. U.L. Ifeanyichukwu, O.E. Fayemi, C.N. Ateba, *Molecules* **25**, No 19, 4521 (2020).
44. R.V. Hernández, M.A.A. Lemus, S. De la Rosa García, R.L. González, P. Quintana, D.G. Zaleta, S.G. Cornelio, *Nanomaterials* **14** No 12, 1007 (2024).
45. S.S. Sana, D.V. Kumbhakar, A. Pasha, S.C. Pawar, A.N. Grace, R.P. Singh, W. Peng, *Molecules* **25** No 21, 4896 (2020).
46. A.S. Abdelbaky, T.A. Abd El-Mageed, A.O. Babalghith, S. Selim, A.M. Mohamed, *Antioxidants* **11** No 8, 1444 (2022).
47. G. Nagaraju, H. Nagabhushana, D. Suresh, C. Anupama, G.K. Raghu, S.C. Sharma, *Ceram. Int.* **43** No 15, 11656 (2017).
48. P.A. Luque, O. Nava, G. Romo-Cardenas, J.I. Nieto-Hipolito, A.R. Vilchis-Nestor, K. Valdez, F.N. Murrieta-Rico, *IEEE Sens. J.* **21** No 10, 11275 (2020).
49. S.Ş. Doğan, A. Kocabaş, *Hum. Exp. Toxicol.* **39** No 3, 319 (2020).
50. R. Álvarez-Chimal, V.I. García-Pérez, M.A. Álvarez-Pérez, J.Á. Arenas-Alatorre, *Mater. Sci. Eng. C.* **118**, 111540 (2021).
51. S.M.H. Akhter, Z. Mahmood, S. Ahmad, F. Mohammad, *BioNanoSci.* **8** No 3, 811 (2018).
52. H. Sadiq, F. Sher, S. Sehar, E.C. Lima, S. Zhang, H.M. Iqbal, M. Nuhanović, *J. Mol. Liq.* **335**, 116567 (2021).
53. S.K. Chaudhuri, L. Malodia, *Appl. Nanosci.* **7** No 8, 501 (2017).
54. A.K. Tiwari, S. Jha, S.K. Tripathi, R. Shukla, R.R. Awasthi, A.K. Bhardwaj, A. Dikshit, *Discov. Appl. Sci.* **6** No 8, 399 (2024).
55. M.A. Ansari, M. Murali, D. Prasad, M.A. Alzohairy, A. Almatroudi, M.N. Alomary, S.R. Niranjana, *Biomolecules* **10** No 2, 336 (2020).
56. C. Ragavendran, M. Imath, C. Kamaraj, I. Nakouti,

- S. Manoharadas, *Mol. Biol. Rep.* **51**, 1128 (2024).  
57. S.V. Gudkov, D.E. Burmistrov, D.A. Serov, M.B. Rebezov, A.A. Semenova, A.B. Lisitsyn, *Front. Phys.* **9**, 641481 (2021).  
58. F.S. Youssef, S.H. Ismail, O.A. Fouad, G.G. Mohamed, *Egypt. J. Vet. Sci.* **55** No 1, 287 (2024).  
59. F. Islam, S. Shohag, M.J. Uddin, M.R. Islam, M.H. Nafady, A. Akter, S. Cavalu, *Materials* **15** No 6, 2160 (2022).  
60. E.L. Irede, R.F. Awoyemi, B. Owolabi, O.R. Aworinde, R.O. Kajola, A. Hazeer, I. H. Ifijen, *RSC Adv.* **14** No 29, 20992 (2024).

### **Зелений синтез ZnO-наночастинок із використанням листових екстрактів лікарських деревних рослин Того, їх характеристика та антимікробні застосування**

Е.С. Адеуї<sup>1</sup>, К. Сесіме<sup>1</sup>, А.Д. Хоунсі<sup>1</sup>, П. Піссан<sup>2</sup>, С.А.С. Бону<sup>3</sup>, К.Ж.Б. Амевоуте<sup>1</sup>, М. Агбахунгбата<sup>3</sup>,  
М.М. Дзаглі<sup>1,4</sup>, В.А. Адедеджі<sup>5</sup>, А.К. Айї<sup>6</sup>, М.А. Мохоу<sup>1</sup>

<sup>1</sup> Лабораторія LPMCS, факультет наук, Університет Ломе, 01BP1515 Ломе, Того

<sup>2</sup> Лабораторія LaSBASE, ESTBA, Університет Ломе, 01BP1515 Ломе, Того

<sup>3</sup> Лабораторія рентгенівських методів / Агентство розвитку Seme City X-TechLab, Семе, Бенін

<sup>4</sup> Регіональний центр передового досвіду з електротехніки, Університет Ломе, 01BP1515 Ломе, Того

<sup>5</sup> Державний університет Елізабет-Сіті, США

<sup>6</sup> Університет Оуберн, Національна коаліція незалежних науковців, США

Тропічні інфекційні захворювання все частіше демонструють резистентність до антибіотиків. Одним зі шляхів боротьби з цією проблемою є інтеграція наночастинок у лікарські засоби. Цинкооксидні наночастинок (ZnONPs) мають виражені антимікробні властивості, а їх синтез із застосуванням лікарських рослин є екологічним та економічно вигідним. У дослідженні використано листові екстракти трьох традиційно лікарських рослин Того — *Newbouldia Leavis*, *Launaea Taraxacifolia* та *Combretum Micranthum* — як відновлювальні та стабілізуювальні агенти у процесі біосинтезу ZnONPs. Проведено дослідження структурних та оптичних властивостей наночастинок за допомогою: UV-Vis спектроскопії, флуоресценції, рентгеноструктурного аналізу (XRD), сканувальної електронної мікроскопії (SEM), енергетично-дисперсійної спектроскопії (EDS). Основні результати: Поглинання в діапазоні 370–377 нм, Флуоресценція при збудженні 365 нм у межах 450–700 нм, Рентгеноструктурний аналіз підтвердив гексагональну структуру вюрциту з розміром кристалітів 39,05 нм, SEM показав агломерацію наноструктур, EDS підтвердив наявність оксиду цинку. Антимікробні тести проти *S. Aureus* і *E. Coli* продемонстрували виразні зони інгібування, що свідчить про ефективність ZnONPs. Таким чином, зелений синтез на основі рослин підвищує біомедичні властивості ZnONPs і відкриває перспективний шлях їх застосування в наномедицині.

**Ключові слова:** ZnO-наночастинок, Зелений синтез, Структурна та оптична характеристика, Антимікробне застосування.